THE ASTROPHYSICAL JOURNAL, 559:572–583, 2001 October 1

PROBING THE CORE STRUCTURE OF DARK HALOS WITH TANGENTIAL AND RADIAL ARC STATISTICS

MASAMUNE OGURI, ATSUSHI TARUYA,[1] AND YASUSHI SUTO[1]
Department of Physics, School of Science, University of Tokyo, 7-3-1 Hongo, Bunkyo-ku, Tokyo 113-0033, Japan; oguri@utap.phys.s.u-tokyo.ac.jp, ataruya@utap.phys.s.u-tokyo.ac.jp, suto@phys.s.u-tokyo.ac.jp
Received 2001 May 15; accepted 2001 June 11

ABSTRACT

We study the arc statistics of gravitational lensing generated by dark matter halos in order to probe their density profile. We characterize the halo profile by two parameters, the inner slope of the central cusp α and the median amplitude of the concentration parameter, $c_{\rm norm}$, for a halo of mass $10^{14}\ h^{-1}\ M_\odot$ at $z = 0$ and compute the numbers of tangential and radial arcs produced by gravitational lensing of galaxy clusters. We find that the number of arcs divided by the number of halos is a good statistic that is sensitive to both $c_{\rm norm}$ and α with very weak dependence on the cosmological parameters. If arc samples with well-defined selection criteria for the clusters become available, one can strongly constrain both $c_{\rm norm}$ and α. While our tentative comparison with the existing observational data indicates that the inner density profile of dark halos is indeed as steep as predicted by recent simulations ($\alpha \sim 1.5$), homogeneous samples of tangential and radial arcs are required for more quantitative discussions.

Subject headings: cosmology: theory — dark matter — galaxies: clusters: general — galaxies: halos — gravitational lensing

1. INTRODUCTION

Dark matter halos play a central role in the standard picture of the cosmological structure formation as plausible sites hosting a variety of astronomical objects, such as galaxies and clusters of galaxies. On the basis of a series of systematic cosmological N-body simulations, Navarro, Frenk, & White (1996, 1997; hereafter collectively NFW) found that the density profile obeys the "universal" form $\rho(r) \propto r^{-1}(r + r_s)^{-2}$ irrespective of the underlying cosmological parameters, the shape of the primordial fluctuation spectrum, and the formation histories. More recent high-resolution simulations indeed confirmed the existence of the central cusp but suggested an even steeper inner slope, $\rho(r) \propto r^{-1.5}$, rather than $\propto r^{-1}$ (Moore et al. 1999; Fukushige & Makino 2001). Nevertheless, the universality of the profiles in numerical simulations is fairly well established except for the possible weak dependence on the halo mass (Jing & Suto 2000) and also some scatter around the mean (Jing 2000).

The above indications from simulations, however, do not seem to be supported by either simple theoretical considerations or available observations. Plausible theoretical models rather predict that the inner slope of the halo profile should depend on the primordial fluctuation spectrum (Hoffman & Shaham 1985; Syer & White 1998) and also on the merger history (Nusser & Sheth 1999; see also Łokas & Hoffman 2000). Detailed analyses of the X-ray surface brightness of clusters of galaxies (Wu & Xue 2000; Wu & Chiueh 2001) are inconsistent with the scaling of the halo concentration against the halo mass predicted by simulations. Furthermore, the rotation curves of both the low surface brightness galaxies (Salucci & Burkert 2000; de Blok et al. 2001) and the inner region of the cluster Cl 0024+1654, reconstructed from gravitational lensing images (Tyson, Kochanski, & Dell'Antonio 1998), indicate a flat core instead of a central cusp, although some controversy about each claim still remains (van den Bosch et al. 2000; Broadhurst et al. 2000; Shapiro & Iliev 2000). This conflict has motivated wild proposals, including an idea that dark matter is self-interacting (Spergel & Steinhardt 2000).

Since the current situation concerning the numerical, theoretical, and observational indications for dark matter halo profiles is somewhat puzzling, it is important to develop another independent methodology to probe the profiles. For this purpose, we focus on the arc statistics of the gravitational lensing in the present paper. The major advantages of this methodology include the following: (1) gravitational lensing offers us a direct route to the mass distribution of the dark halo without additional assumptions, for instance, about the physical conditions of gas and stars; (2) the gravitational arcs are produced mainly because of galaxy clusters, which have an empirically good one-to-one correspondence with dark halos, in marked contrast with the case of multiple QSO images due to galaxies (Nakamura & Suto 1997; Li & Ostriker 2001; Wyithe, Turner, & Spergel 2001; Keeton & Madau 2001; Takahashi & Chiba 2001); and (3) observational confrontation for an individual object may suffer from the specific selection function and the scatter from the mean profile, and thus the statistical average over the cosmological volume is important.

Several authors have already examined the effect of the inner profile of dark halos on giant luminous arcs (Wu & Hammer 1993; Miralda-Escudé 1993a, 1993b; Hamana & Futamase 1997; Hattori, Watanabe, & Yamashita 1997; Williams, Navarro, & Bartelmann 1999; Molikawa et al. 1999; Meneghetti et al. 2001). In particular, Bartelmann et al. (1998) suggested a strong dependence of arc statistics on cosmological parameters because of the different core structure of dark halos for different cosmological models. Keeton & Madau (2001) found that the number of predicted lenses is strongly correlated with core mass fraction, which results in a strong degeneracy between the inner slope of the central cusp and the dark matter concentration. Molikawa & Hattori (2001) pointed out that the number ratio of tangential and radial arcs produced by a given cluster is

[1] Also at Research Center for the Early Universe (RESCEU), School of Science, University of Tokyo, Tokyo 113-0033, Japan.

tightly correlated with the inner slope: on the basis of 11 tangential and three radial arcs for six clusters, they conclude that the central cusp $\propto r^{-1.5}$ is indeed favored. Although the existing samples of clusters are somewhat heterogeneous and do not satisfy well-defined selection criteria, this indicates that the arc statistics become useful probes of the core structure of the dark halos. Therefore, we present a first systematic study of the effects of the dark halo profiles on the gravitational tangential and radial arc statistics. In particular, we take proper account of the magnification bias, the finite size of the source galaxies, and the luminosity distribution and evolution of source galaxies.

The rest of the paper is organized as follows: Section 2 briefly summarizes the main properties of the generalized NFW profile, and § 3 presents an analytic formalism of the number count of arcs. Our predictions for the arc statistics are shown in § 4. Finally, we summarize the conclusions and discuss further implications in § 5.

2. DESCRIPTION OF THE DENSITY PROFILES OF DARK MATTER HALOS

2.1. *Generalized NFW Profile*

Throughout the paper, we adopt a generalized NFW profile for dark matter halos of the form (Jing & Suto 2000)

$$\rho(r) = \frac{\rho_{\rm crit}\,\delta_c}{(r/r_s)^{\alpha}(1 + r/r_s)^{3-\alpha}}\,, \tag{1}$$

where r_s is a scale radius and δ_c is a characteristic density. The profile with $\alpha = 1$ corresponds to the one NFW proposed, and that with $\alpha = 1.5$ agrees with the inner profile claimed by Moore et al. (1999) and Fukushige & Makino (2001). The shape of halos is also characterized by the concentration parameter, which is defined as the ratio of the size of the halo to the scaled radius r_s. Originally NFW used r_{200}, the halo radius where the mean inner density reaches 200 times the critical density of the universe. Rather, we follow Bullock et al. (2001) and adopt the definition

$$c_{\rm vir}(M_{\rm vir}) \equiv \frac{r_{\rm vir}(M_{\rm vir})}{r_s(M_{\rm vir})}\,. \tag{2}$$

The virial radius, $r_{\rm vir}$, in the above expression is defined through the overdensity $\Delta_{\rm vir}$ at the virialization epoch $z_{\rm vir}$ as

$$M_{\rm vir} = \frac{4\pi}{3}\,\Delta_{\rm vir}\,\bar{\rho}(z_{\rm vir}) r_{\rm vir}^3\,, \tag{3}$$

where $\bar{\rho}(z_{\rm vir})$ denotes the mean density of the universe at virialization. Once the density parameter Ω_0 and the cosmological constant λ_0 are specified, the value of $\Delta_{\rm vir}$ can be computed using the nonlinear spherical collapse model. We use the following formulae:

$$\Delta_{\rm vir} = \begin{cases} 4\pi^2\,\dfrac{(\cosh\eta_{\rm vir} - 1)^3}{(\sinh\eta_{\rm vir} - \eta_{\rm vir})^2}\,, & \text{if } (\Omega_0 < 1,\ \lambda_0 = 0)\,, \\ 18\pi^2(1 + 0.4093\omega_{\rm vir}^{0.9052}), & \text{if } (\Omega_0 < 1,\ \lambda_0 = 1 - \Omega_0)\,, \end{cases} \tag{4}$$

where $\eta_{\rm vir} \equiv \cosh^{-1}(2/\Omega_{\rm vir} - 1)$, $\omega_{\rm vir} \equiv 1/\Omega_{\rm vir} - 1$, and the density parameter at virialization is

$$\Omega_{\rm vir} = \frac{\Omega_0(1 + z_{\rm vir})^3}{\Omega_0(1 + z_{\rm vir})^3 + (1 - \Omega_0 - \lambda_0)(1 + z_{\rm vir})^2 + \lambda_0}\,. \tag{5}$$

The approximation to $\Delta_{\rm vir}$ in equation (4) for $\lambda_0 = 1 - \Omega_0$ was obtained by Kitayama & Suto (1996).

Equations (1) and (3) imply that the characteristic density δ_c is related to the concentration parameter $c_{\rm vir}$ as

$$\delta_c = \frac{\Delta_{\rm vir}\,\Omega_{\rm vir}}{3}\,\frac{c_{\rm vir}^3}{A(c_{\rm vir})}\,, \tag{6}$$

where $A(c_{\rm vir})$ is

$$A(c_{\rm vir}) = \frac{c_{\rm vir}^{3-\alpha}}{3 - \alpha}\,{}_2F_1(3 - \alpha, 3 - \alpha; 4 - \alpha; -c_{\rm vir})\,, \tag{7}$$

with ${}_2F_1(a, b; c; x)$ being the hypergeometric function (e.g., Keeton & Madau 2001).

2.2. *Concentration Parameter*

Navarro et al. (1997) and Bullock et al. (2001) have extensively examined the cosmological model dependence and redshift evolution of the concentration parameter from N-body simulations, adopting the profile in equation (1) with $\alpha = 1$. Since we consider models with $\alpha \neq 1$ as well, we have to generalize their results. For this purpose, we follow Keeton & Madau (2001). They first define the radius r_{-2} at which the logarithmic slope of the density profile is -2, i.e., $d\ln\rho/d\ln r = -2$. For the profile of equation (1), $r_{-2} = (2 - \alpha)r_s$, and thus the corresponding concentration parameter reduces to

$$c_{-2} \equiv \frac{r_{\rm vir}}{r_{-2}} = \frac{1}{2 - \alpha}\,c_{\rm vir}\,. \tag{8}$$

Then they point out the importance of the scatter of the concentration parameter (Jing 2000; Bullock et al. 2001) on the lensing statistics and model the probability distribution function of c_{-2} as a lognormal function:

$$p(c_{-2})dc_{-2} = \frac{1}{\sqrt{2\pi}\sigma_c} \exp\left[-\frac{(\ln c_{-2} - \ln c_{-2,\mathrm{median}})^2}{2\sigma_c^2}\right] d\ln c_{-2} \tag{9}$$

with $\sigma_c = 0.18$. Jing (2000) reported that this dispersion is fairly insensitive to the cosmological model parameters. Finally, we introduce the scaling of $c_{-2,\mathrm{median}}$ according to the simulations by Bullock et al. (2001):

$$c_{-2,\mathrm{median}} = c_{\mathrm{norm}} \frac{1}{1+z} \left(\frac{M_{\mathrm{vir}}}{10^{14}\, h^{-1}\, M_\odot}\right)^{-0.13}, \tag{10}$$

where h denotes the Hubble constant in units of 100 km s^{-1} Mpc^{-1}. Bullock et al. (2001) estimate $c_{\mathrm{norm}} \sim 8$ from their simulations with $(\Omega_0, \lambda_0) = (0.3, 0.7)$. In the statistical analyses presented below, we parameterize the halo profiles by the amplitude c_{norm} and the inner slope α, assuming that the above description is applicable equally well to the three cosmological models that we consider.

3. TANGENTIAL AND RADIAL ARC STATISTICS

3.1. *Lens Equations*

We denote the image position in the lens plane by $\boldsymbol{\xi}$ and the source position in the source plane by $\boldsymbol{\eta}$. For the spherical symmetric profile (equation [1]), the lens equation (e.g., Schneider, Ehlers, & Falco 1992) reduces to

$$y = x - bf(x), \tag{11}$$

where $x = |\boldsymbol{\xi}|/r_s$, $y = |\boldsymbol{\eta}|\, D_{OL}/r_s D_{OS}$, and D_{OL} and D_{OS} denote the angular diameter distances from the observer to the lens and the source planes, respectively. The factors b and $f(x)$ are related to the dark halo profile as follows:

$$b = \frac{4\rho_{\mathrm{crit}}\, \delta_c\, r_s}{\Sigma_{\mathrm{crit}}}, \tag{12}$$

$$f(x) = \frac{1}{x}\int_0^\infty dz \int_0^x dx' \frac{x'}{(\sqrt{x'^2+z^2})^\alpha (1+\sqrt{x'^2+z^2})^{3-\alpha}}, \tag{13}$$

where Σ_{crit} is the critical surface mass density:

$$\Sigma_{\mathrm{crit}} = \frac{c^2}{4\pi G}\frac{D_{OS}}{D_{OL} D_{LS}}. \tag{14}$$

3.2. *Number of Arcs per Halo*

We consider the distortion of images of source galaxies due to the spherical halo lensing, neglecting the intrinsic ellipticity of those galaxies. In this case the tangential and radial stretching factors of a source image at the source position x with respect to the center of the lens halo are simply given by $\mu_t(x) \equiv (y/x)^{-1}$ and $\mu_r(x) \equiv (dy/dx)^{-1}$ because of the spherical symmetry of halos. In terms of these, we define the tangential and radial arcs as those satisfying

$$T(x) = \left|\frac{\mu_t(x)}{\mu_r(x)}\right| > \epsilon_{\mathrm{th}} \qquad \text{(tangential arc)}, \tag{15}$$

$$R(x) = \left|\frac{\mu_r(x)}{\mu_t(x)}\right| > \epsilon_{\mathrm{th}} \qquad \text{(radial arc)}. \tag{16}$$

We adopt $\epsilon_{\mathrm{th}} = 4$ for the threshold of the length-to-width ratio. This value is different from the canonical threshold for giant luminous arcs, $\epsilon_{\mathrm{th}} = 10$, adopted by Wu & Hammer (1993), because most radial arcs presently observed have a rather small length-to-width ratio.

The projected areas around a given halo of mass M at z_L satisfying equations (15) and (16) yield the cross sections $\sigma(M, z_L, z_S)$ for tangential and radial arcs of circular galaxies located at z_S, respectively. Actually, the above definition ignores the finite size of the source galaxies. If the size of the area on the source plane, $\Delta\eta$, satisfying condition (15) or (16) is smaller than that of source, however, observable arcs are not produced (see, e.g., Schneider et al. 1992). Since the smallest galaxy size that is observed as an arc (Hattori et al. 1997) roughly corresponds to $\eta_{\mathrm{crit}} = 1\, h^{-1}$ kpc, we set $\sigma(M, z_L, z_S) = 0$ for $\Delta\eta < \eta_{\mathrm{crit}}$.

Figure 1 shows the lensing cross sections for tangential and radial arcs as a function of source redshift z_S. We present the cases in which the mass of the lens halo is $M = 10^{15}\, h^{-1}\, M_\odot$ and $M = 5 \times 10^{15}\, h^{-1}\, M_\odot$, because radial arcs are not formed for $M \sim 10^{14}\, h^{-1}\, M_\odot$ unless α or c_{norm} is unrealistically large. The redshift of the lens halo is fixed at $z_L = 0.2$. These plots show that the lensing cross section significantly increases as α or c_{norm}, or both, becomes larger. Furthermore, the cross sections for tangential and radial arcs depend on these two parameters rather differently. In turn, separate consideration of tangential and radial arcs yields useful constraints on the core structure of dark halos.

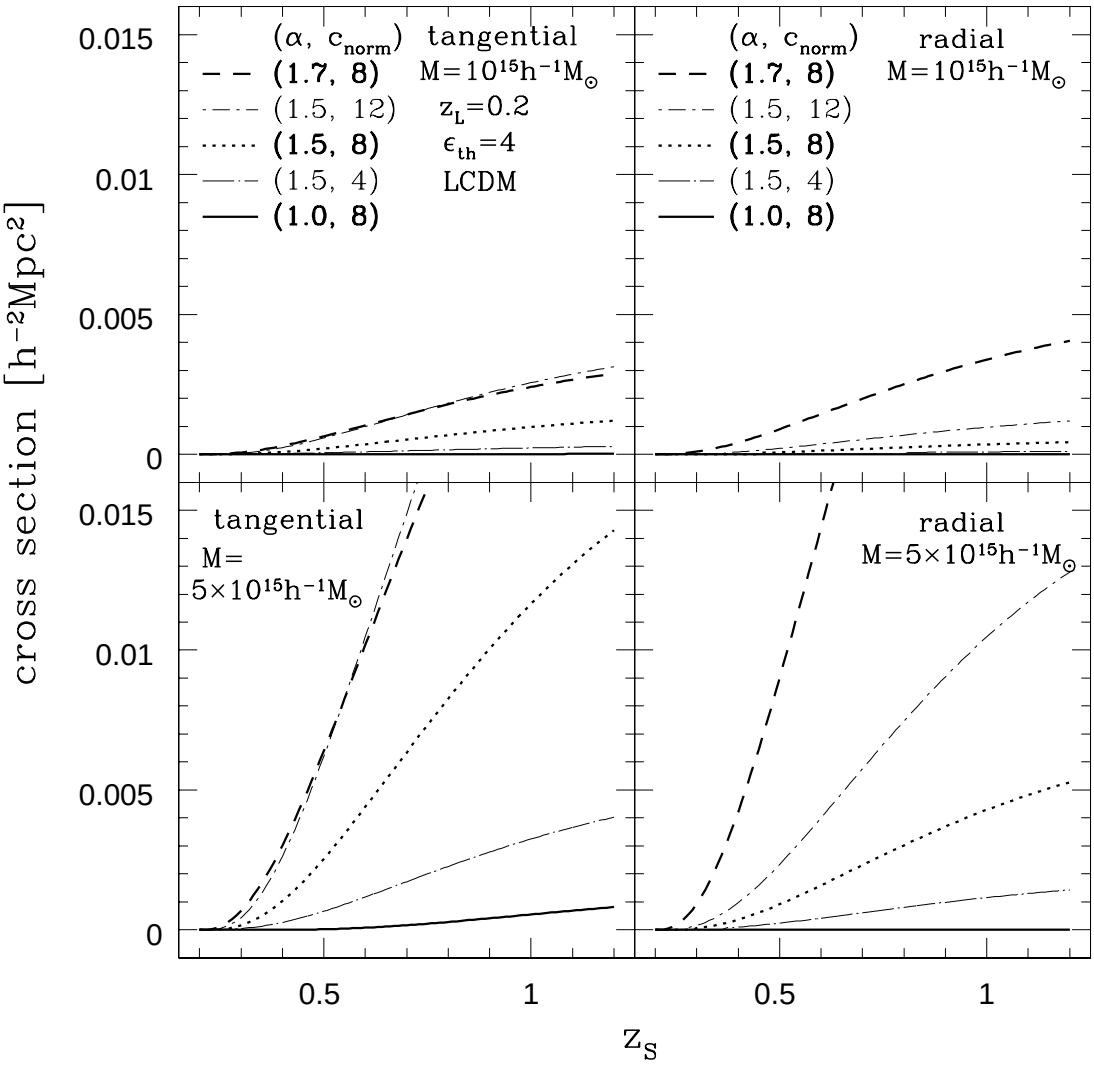

FIG. 1.—Lensing cross sections for tangential (*left*) and radial (*right*) arcs against the source redshift z_S for an $\Omega_0 = 0.3$ and $\lambda_0 = 0.7$ model. The redshift of the lensing halo is fixed at $z_L = 0.2$. Different lines correspond to the different sets of α and $c_{\rm norm}$. Top and bottom panels indicate the results for halo masses of 10^{15} and $5 \times 10^{15}\ h^{-1}\ M_\odot$, respectively.

Once the relevant cross section is computed, one can calculate the number of arcs produced by a halo of mass M at redshift z_L:

$$N(M, z_L) = \int_{z_L}^{z_{S,\max}} dz_S\, \sigma(M, z_L, z_S)\, \frac{c\, dt}{dz_S}\, (1 + z_S)^3 \int_{L_{\min}}^{\infty} dL\, n_g(L, z_S)\,, \tag{17}$$

where $\sigma(M, z_L, z_S)$ is the tangential or radial cross section in the source plane, $c\, dt/dz_S$ denotes the proper differential distance at z_S,

$$\frac{c\, dt}{dz_S} = \frac{c}{H_0}\, \frac{1}{(1 + z_S)\sqrt{\Omega_0(1 + z_S)^3 + (1 - \Omega_0 - \lambda_0)(1 + z_S)^2 + \lambda_0}}\,, \tag{18}$$

and $n_g(L, z_S)$ denotes the luminosity function of source galaxies.

We incorporate the redshift evolution of the luminosity function of galaxies for $z \lesssim 1$, adopting the empirical fit by Broadhurst, Ellis, & Shanks (1988):

$$\log\, \phi(L, z) = \log\, \phi(L, 0) + (0.1z + 0.2z^2) \log \left[\frac{\phi(L, 0)}{\phi(L_{\max}, 0)}\right], \tag{19}$$

where $L_{\max}$ is the bright-end luminosity corresponding to $M_{\max} = -22.0 + 5 \log h$. Therefore, we have to restrict our consideration for source galaxies up to $z_{S,\max} = 1$.

For the local luminosity function $\phi(L, 0)$, we use the Schechter function normalized to the Two Degree Field (2dF) galaxy redshift survey:

$$\phi(L, 0)dL = \phi^*\left(\frac{L}{L^*}\right)^{\alpha} \exp\left(-\frac{L}{L^*}\right)\frac{dL}{L^*}, \tag{20}$$

where $\phi^* = 0.0169\ h^{-3}$ Mpc^3, $\alpha = -1.28$, and $M^* = -19.73 + 5 \log h$ (Folkes et al. 1999). While those values are derived assuming $\Omega_0 = 1$, we compute the values in different cosmological models by applying an appropriate scaling so that the observed galaxy number counts versus their flux is unchanged.

To evaluate equation (17), we also need the lower bound of the luminosity, $L_{\rm min}$, which depends on the magnification of arcs and the limiting magnitude of the sample. First, the magnification of arcs becomes

$$\mu(x) = |\mu_t(x)\mu_r(x)| = T(x)\{\mu_r(x)\}^2 = R(x)\{\mu_t(x)\}^2, \tag{21}$$

where x denotes the position of arcs in the lens plane. The quantity μ formally diverges in the case of a point source. In practice, however, $\mu(x)$ saturates at about the value that corresponds to the value of the position deviating from the critical curve by the source size (e.g., Schneider et al. 1992). Therefore, we assume that all arcs are magnified by a factor of $\epsilon_{\rm th}\{\mu_r(x_t)\}^2$ for tangential arcs and $\epsilon_{\rm th}\{\mu_t(x_r)\}^2$ for radial arcs, where x_t and x_r are the position of tangential and radial critical curves. Second, we use $m_B < 26.5$ as the B-band limiting magnitude of the arc observation. The apparent magnitude can be translated to the luminosity if we employ the K-correction in B-band,

$$K(z) = -0.05 + 2.35z + 2.55z^2 - 4.89z^3 + 1.85z^4, \tag{22}$$

for spiral galaxies (King & Ellis 1985). Taking both effects into account, $L_{\rm min}$ becomes

$$\frac{L_{\rm min}}{L^*} = \frac{10^{-0.4(m_{B,\max} - m^*)}}{\epsilon_{\rm th}\{\mu_r(x_t)\}^2}, \tag{23}$$

$$m^* = M^* + 5 \log\left[\frac{D_{\rm lum}(z_S)}{10\ {\rm pc}}\right] + K(z_S), \tag{24}$$

in the case of tangential arcs, where $D_{\rm lum}$ is the luminosity distance.

3.3. *Total Number of Arcs*

Finally, we calculate the total number of arcs by integrating equation (17) as

$$N_{\rm tot} = \int_{z_{L,\min}}^{z_{L,\max}} dz_L \int_{M_{\rm min}(z_L)}^{\infty} dM\, N(M, z_L)\, n_{\rm PS}(M, z_L)(1 + z_L)^3 4\pi D_{OL}^2 \frac{c\, dt}{dz_L}, \tag{25}$$

where $n_{\rm PS}$ is the comoving number density of halos. We use the Press-Schechter mass function (Press & Schechter 1974):

$$n_{\rm PS}(M, z) = \sqrt{\frac{2}{\pi}}\frac{\bar{\rho}(z=0)}{M}\frac{\delta_0(z)}{\sigma_M^2}\left|\frac{d\sigma_M}{dM}\right| \exp\left[-\frac{\delta_0^2(z)}{2\sigma_M^2}\right], \tag{26}$$

where σ_M is the rms linear density fluctuation on mass scale M at $z = 0$ and $\delta_0(z)$ is the critical linear density contrast, given by

$$\delta_0(z) = \frac{3}{20}\frac{(12\pi)^{2/3}}{D(z)}, \tag{27}$$

with $D(z)$ being the linear growth rate normalized to unity at $z = 0$. We consider two selection functions, i.e., the minimum mass of integration $M_{\rm min}(z_L)$ for definiteness: the first adopts a constant minimum mass independent of z_L, and the other corresponds to an X-ray survey with a surface brightness flux limit of $S_{\rm min}$. Throughout the paper, we use the 0.5–2.0 keV band for the flux. Assuming the conventional one-to-one correspondence between dark halos and X-ray clusters, one can relate $M_{\rm min}(z_L)$ to $S_{\rm min}$, and we use the relation shown in Suto et al. (2000).

4. RESULTS

4.1. *Number Counts of Arcs*

In the specific examples presented below, we consider three representative cosmological models dominated by cold dark matter (CDM), lambda CDM (LCDM), standard CDM (SCDM), and open CDM (OCDM), with $(\Omega_0, \lambda_0, h, \sigma_8) = (0.3, 0.7, 0.7, 1.04)$, $(1.0, 0.0, 0.5, 0.56)$, and $(0.45, 0.0, 0.7, 0.83)$, respectively. The amplitude of the mass fluctuation, σ_8, smoothed over a top-hat radius of $8\ h^{-1}$ Mpc, is normalized so as to reproduce the X-ray luminosity and temperature functions of clusters (Kitayama & Suto 1997).

Figure 2 plots the number of halos per steradian (*top*), tangential arcs (*middle*), and radial arcs (*bottom*) between $z_L - \Delta z_L/2$ and $z_L + \Delta z_L/2$ with $\Delta z_L = 0.05$ for $\alpha = 1.5$, $c_{\rm norm} = 8$, and $z_S < 1$. The triangles, squares, and circles indicate the results for LCDM, SCDM, and OCDM. The numbers of arcs in the middle and bottom panels are divided by the number of halos plotted in the top panels. The left and right panels correspond to the X-ray flux–limited ($S_{\rm lim} = 10^{-13}$ ergs s^{-1} cm^{-2}) and the mass-limited ($M_{\rm min} = 5 \times 10^{14}\ h^{-1}\ M_\odot$) samples. For a given mass and profile of a halo, these plots indicate the range of z_L,

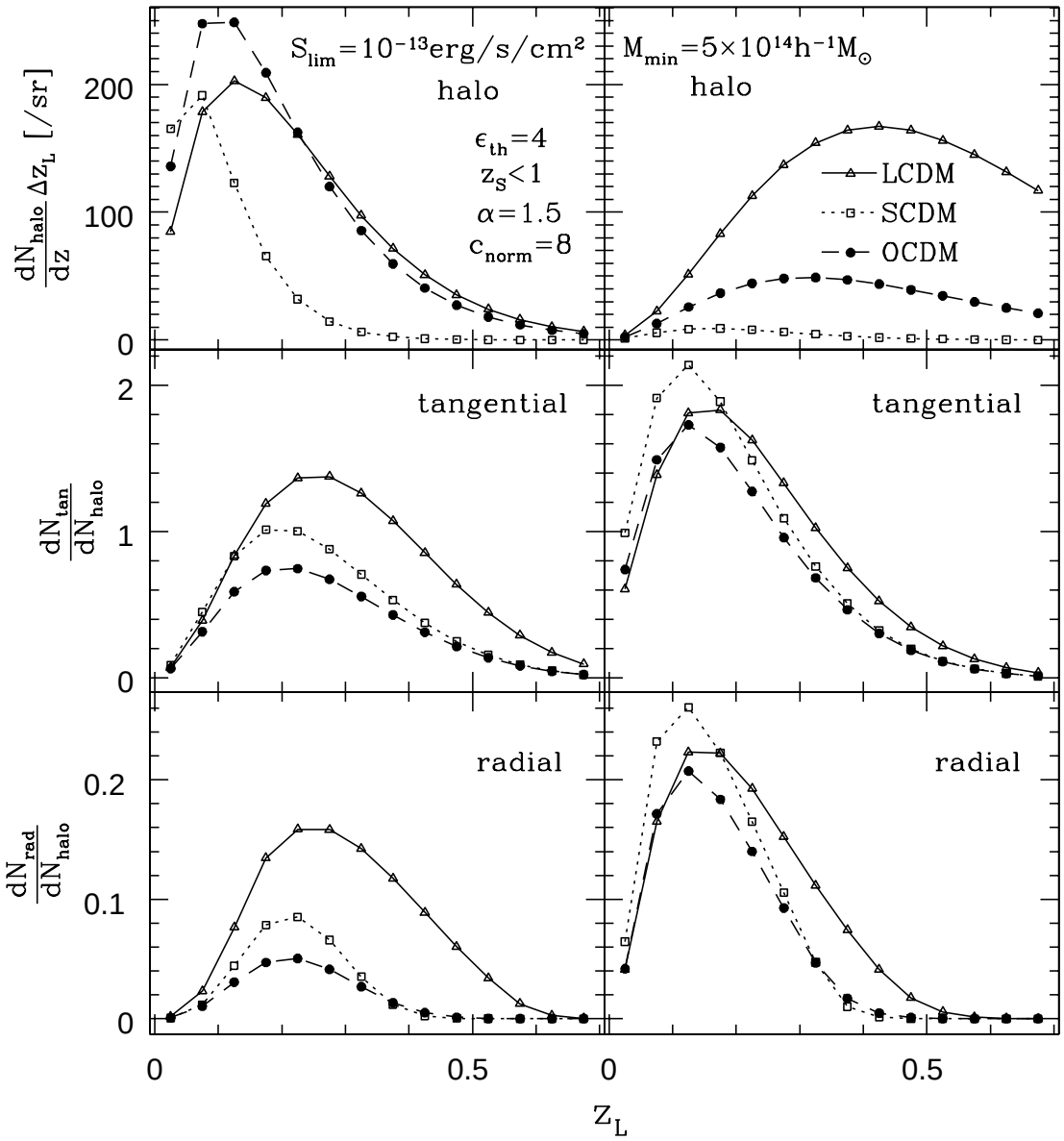

FIG. 2.—Redshift distribution of the numbers of halos per steradian (*top*), tangential arcs (*middle*), and radial arcs (*bottom*). The numbers of tangential and radial arcs in the middle and bottom panels are divided by the number of halos plotted in the top panels. We adopt $\alpha = 1.5$, $c_{\rm norm} = 8$, and $z_S < 1$ and plot those numbers between $z_L - \Delta z_L/2$ and $z_L + \Delta z_L/2$ with $\Delta z_L = 0.05$. Triangles, squares, and circles indicate the results for LCDM, SCDM, and OCDM. The left and right panels correspond to the X-ray flux–limited ($S_{\rm lim} = 10^{-13}$ ergs s^{-1} cm^{-2}) and the mass-limited ($M_{\rm min} = 5 \times 10^{14}\, h^{-1}\, M_\odot$) samples.

that mostly contributes to the formation of arcs. Both tangential and radial arcs are efficiently formed around $z_L \sim 0.2$ and $z_L \sim 0.1$ for fluxlimited and mass-limited samples, respectively.

Note the strong dependence on cosmological parameters. The number of halos per steradian as a function of z_L depends on both the volume of the universe up to z_L and the evolution of the mass function. The former mainly explains why the halos are most abundant in LCDM at higher redshifts, while the latter accounts for earlier declining of halo numbers in SCDM (Fig. 2, *top*). Although this behavior is already well known in the study of cluster abundance (Kitayama, Sasaki, & Suto 1998), we emphasize that the number of arcs *per halo* also increases with the presence of the cosmological constant (Fig. 2, *middle*, *bottom*), as pointed out by Wu & Mao (1996). This comes directly from the dependence of the critical surface mass density (eq. [14]). As plotted in Figure 3, the value of $\Sigma_{\rm crit}$ is smallest in LCDM for a given z_S and z_L, i.e., the lensing probability is largest for a given halo profile. At $z \lesssim 0.1$, SCDM produces more abundant arcs than LCDM because of the higher density of halos for the same halo mass, i.e., $\Delta_{\rm vir}\, \bar{\rho}(z_{\rm vir})$ becomes the largest in the SCDM cosmology (see eq. [4]).

We turn next to the dependence of the halo profiles ($c_{\rm norm}$ and α) on the arc statistics. Figure 4 displays contours of the arc statistics for the flux-limited sample with $S_{\rm lim} = 10^{-13}$ ergs s^{-1} cm^{-2} for LCDM (*top*), SCDM (*middle*), and OCDM (*bottom*). The left and center panels indicate the number of tangential and radial arcs *per halo*, and the right panels plot the number ratio of radial to tangential arcs. Here we integrate equation (25) over lens redshifts of $0.1 < z_L < 0.4$, where arcs are efficiently formed, as discussed above. Clearly both α and $c_{\rm norm}$ significantly influence the arc statistics, an order of magnitude more than the cosmological parameters.

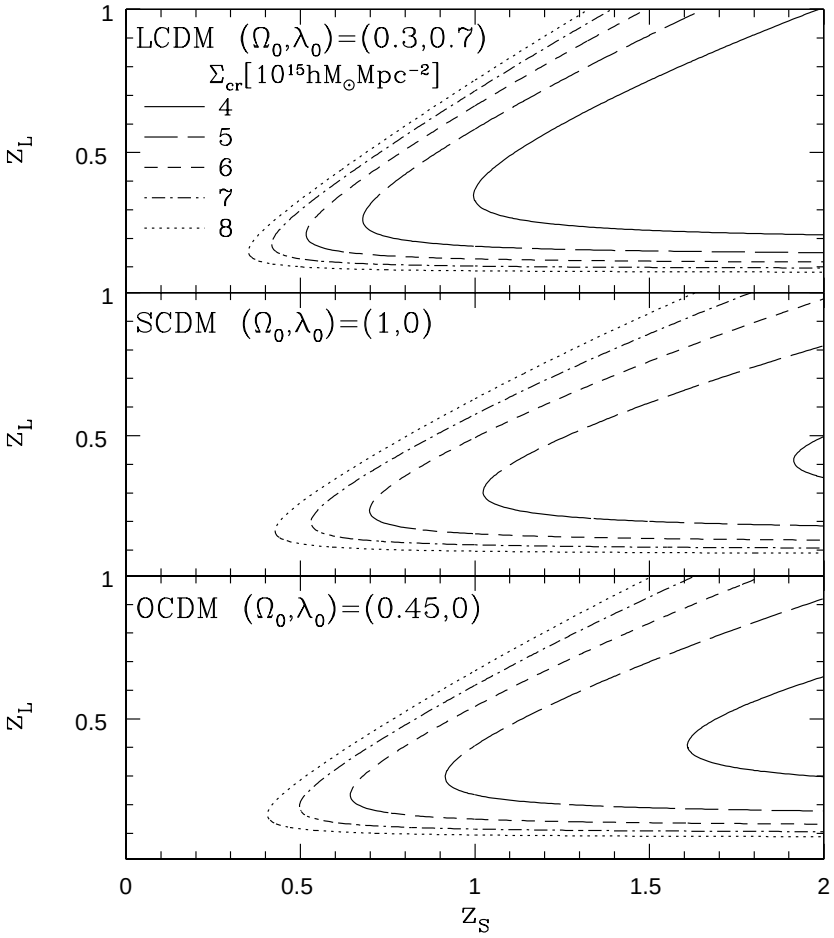

FIG. 3.—Contours of the critical surface density Σ_{crit} on the z_S-z_L plane for three cosmological models: LCDM (*top*), SCDM (*middle*), and OCDM (*bottom*). The contour levels for each line are $\Sigma_{crit} = 4$ (*solid line*), 5 (*long-dashed line*), 6 (*short-dashed line*), 7 (*dash-dotted line*), and 8 (*dotted line*), in units of $10^{15}\, h\, M_\odot$ Mpc^{-2}.

If we use the same statistics,

$$W \equiv \frac{N_{\rm tot,rad}}{N_{\rm tot,tan}}\,, \tag{28}$$

proposed by Molikawa & Hattori (2001) originally for a single cluster, we confirm that the cosmological model dependence is extremely weak even after the statistical average over the redshift. In particular, the number ratio W is not so sensitive to $c_{\rm norm}$ and is basically a powerful indicator of the inner slope of the dark halo profile. The number of tangential arcs per halo, on the other hand, is more sensitive to $c_{\rm norm}$ (Figure 4, *left panels*). Thus, combining both the tangential and radial arc statistics, we can constrain both α and $c_{\rm norm}$ simultaneously.

Next consider the effects of changing the selection criteria of both halos and sources. Figure 5 shows how the selection criterion of lensing halos alters the prediction of arc statistics in the case of LCDM; from top to bottom, $S_{\rm lim} = 10^{-13}$ ergs s^{-1} cm^{-2}, $S_{\rm lim} = 10^{-12}$ ergs s^{-1} cm^{-2}, $M_{\rm min} = 10^{14}\, h^{-1}\, M_\odot$, and $M_{\rm min} = 10^{15}\, h^{-1}\, M_\odot$. While the different selection criteria yield a factor of 500 difference in the number of halos, the arc statistics *per halo* are fairly robust and remain a powerful discriminator of the halo profile. Figure 6 displays the difference in the prediction caused by altering the threshold of the length-to-width ratio for X-ray flux–limited samples, $S_{\rm lim} = 10^{-13}$ ergs s^{-1} cm^{-2}, in LCDM cosmology. As shown in these plots, changing the threshold mainly changes the number of radial arcs and consequently changes the number ratio W drastically. This strong threshold dependence originates from the finite source size effect and is not incorporated properly in Molikawa & Hattori (2001). Therefore, it is clear that the finite size of source galaxies must be considered even in the case of the number ratio W.

4.2. *Uncertainties of the Predictions*

The results presented above are based on a variety of model assumptions, and we would like to examine the extent to which they affect the conclusions. More specifically, we focus on the mass function for dark halos, the size of source galaxies, and the evolution of the luminosity function of source galaxies.

While the Press-Schechter mass function is widely used in various cosmological predictions, recent numerical simulations (e.g., Jenkins et al. 2001) suggest that it underpredicts the massive halos, while it overpredicts the less massive halos. Sheth &

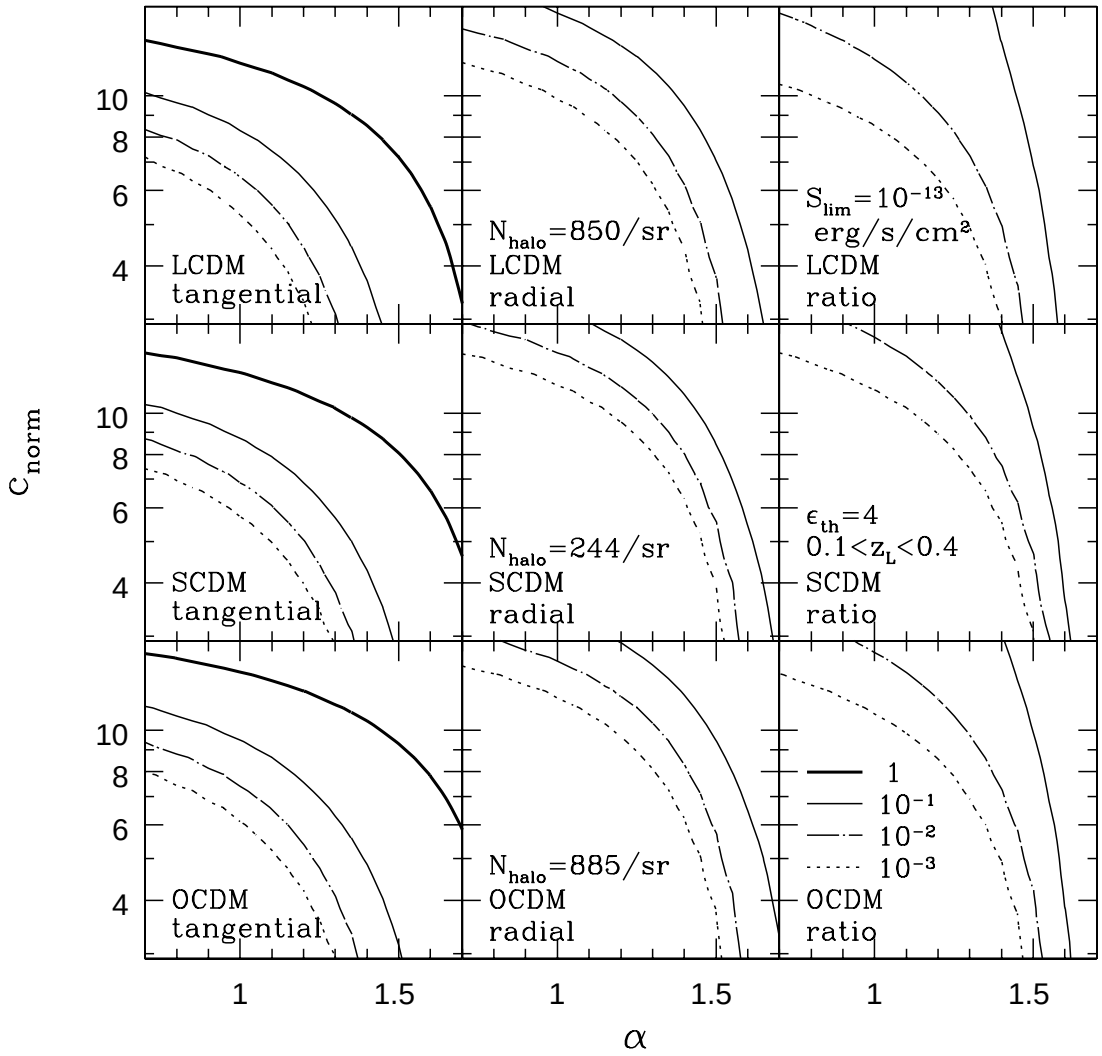

FIG. 4.—Predicted numbers per halo for tangential (*left panels*) and radial (*center panels*) arcs per halo and their ratio $W \equiv N_{\rm tot,rad}/N_{\rm tot,tan}$ (*right panels*) on the α-$c_{\rm norm}$ plane. We consider X-ray flux–limited samples with $S_{\rm lim} = 10^{-13}$ ergs s^{-1} cm^{-2} in three representative cosmological models: LCDM (*top panels*), SCDM (*middle panels*), and OCDM (*bottom panels*). The number of halos $N_{\rm halo}$ is also shown for reference. The contour levels are 1 (*thick solid line*), 10^{-1} (*thin solid line*), 10^{-2} (*dash-dotted line*), and 10^{-3} (*dotted line*).

Tormen (1999) propose an empirical correction for the effect as

$$n_{\rm ST}(M, z) = A\left\{1 + \left[\frac{\sigma_M}{\sqrt{a}\delta_0(z)}\right]^{2p}\right\}\sqrt{\frac{2a}{\pi}}\,\frac{\bar{\rho}(z=0)}{M}\,\frac{\delta_0(z)}{\sigma_M^2}\left|\frac{d\sigma_M}{dM}\right|\,\exp\left[-\frac{a\delta_0^2(z)}{2\sigma_M^2}\right], \tag{29}$$

where $a = 0.707$, $p = 0.3$, and $A = 0.322$. We also consider the cases of a twice-larger threshold for $\eta_{\rm crit} = 2\ h^{-1}$ kpc and a no-evolution luminosity function, i.e., $\phi(L, z) = \phi(L, 0)$. The results separately employing the above change are plotted in Figure 7. Among them only the no-evolution model rather changes the total number of arcs, but this may be too extreme. More importantly, the ratio of the tangential and radial arcs, W, still remains unchanged in practice even if the luminosity evolution is neglected. The twice-larger threshold model mainly changes the number of radial arcs, and as a result this model also changes the number ratio W. Thus, we conclude that the arc statistics presented above are not so affected by the uncertainties of the models and are a fairly robust discriminator of the halo profiles if the finite size of source galaxies is correctly taken into account.

4.3. *Tentative Comparison with Observations*

While there is no homogeneous sample for the arc survey yet available that satisfies our selection criteria, it is tempting to make a comparison with the existing data. Luppino et al. (1999) present the results of an imaging survey for gravitational lensing in a sample of 38 X-ray–selected clusters of galaxies. From these clusters we choose a subsample of 13 clusters that satisfy the conditions $0.1 < z < 0.4$ and $S(0.5\text{–}2.0\ {\rm keV}) > S_{\rm lim} = 10^{-12}$ ergs s^{-1} cm^{-2}. Within these 13 clusters, 15 tangential and two radial arcs with $\epsilon_{\rm th} = 4$ are reported. We attempt to draw cosmological implications by comparing these observational values with our theoretical predictions.

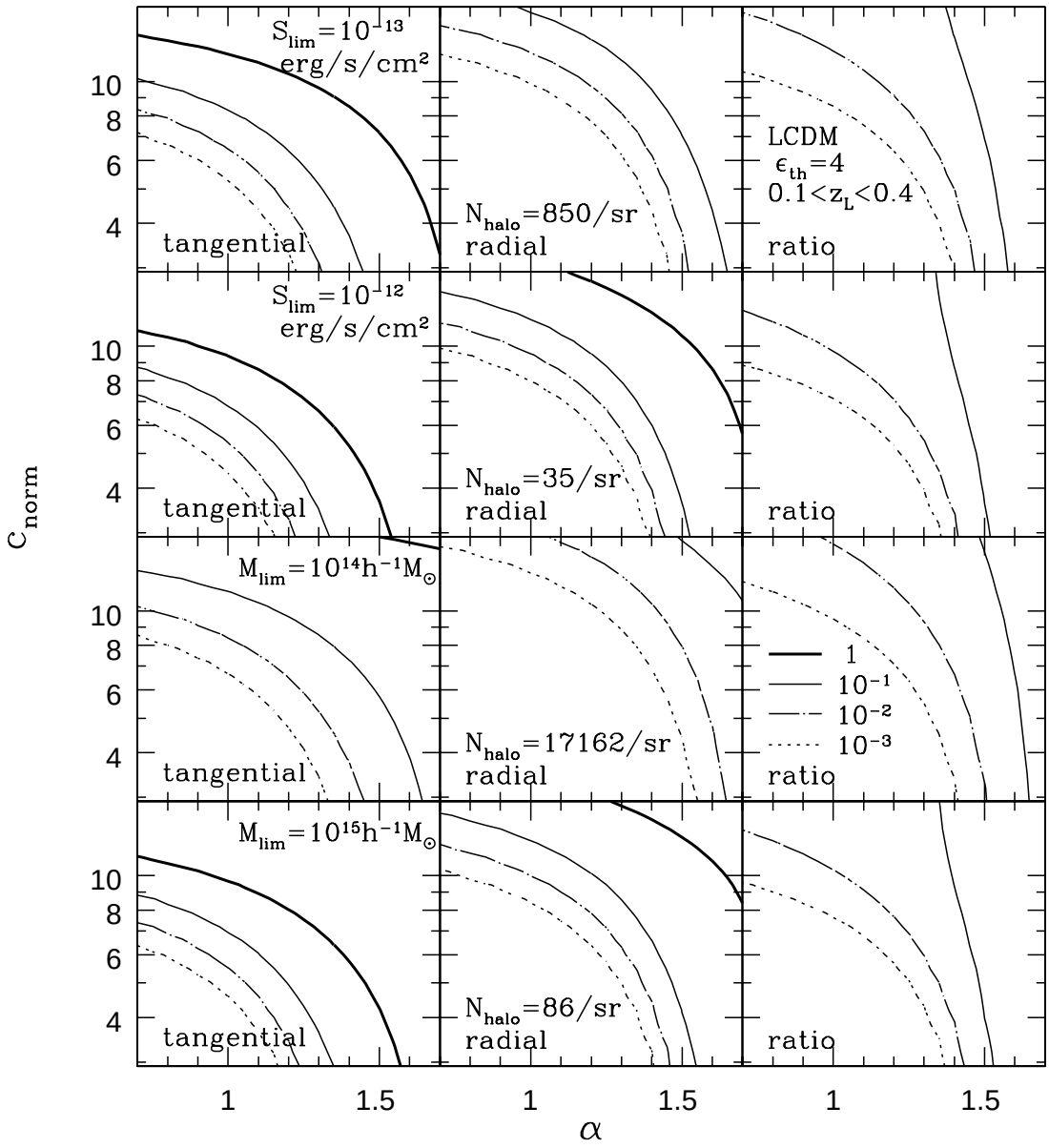

FIG. 5.—Effect of sample selection functions on the arc statistics in the LCDM model. From top to bottom, X-ray flux–limited samples with $S_{lim} = 10^{-13}$ and $S_{lim} = 10^{-12}$ ergs s^{-1} cm^{-2} and mass-limited samples with $M_{min} = 10^{14}$ and $M_{min} = 10^{15}\,h^{-1}\,M_\odot$. The contour levels are the same as in Fig. 4.

Figure 8 shows our tentative comparison with observations, assuming the LCDM cosmology and neglecting possible systematic errors (e.g., intrinsic ellipticities of source galaxies, nonsphericities in lensing halos). This result implies that dark matter halos should have steep inner profiles like those predicted by simulations, $\alpha \sim 1.5$, but rather smaller concentration, $c_{norm} \sim 4$. While it is premature to draw definite conclusions from the present comparison, this analysis clearly exhibits the extent to which our current methodology puts useful constraints on α and c_{norm} separately. Note again that the number of tangential arcs has a strong degeneracy between α and c_{norm}. Thus, it is important to combine the number of tangential arcs with the number ratio W, which is mainly sensitive to α. Although the present example does not exhibit the strong constraint on the concentration parameter c_{norm}, a more severe constraint within $\sim$10% accuracy at the 1 σ level will be obtained if one uses cluster samples of $N_{halo} \sim 100$. This would be achieved irrespective of the cosmological model.

5. DISCUSSION AND CONCLUSIONS

In this paper, we study the arc statistics of gravitational lensing produced by dark matter halos in order to probe their density profile. Adopting the generalized NFW profile (eq. [1]), we describe a statistical method to predict the numbers of tangential and radial arcs as a function of the inner slope α and the concentration parameter c_{norm}. We incorporate several realistic effects, including the magnification bias, the finite size of the source galaxies, and the luminosity distribution and evolution of source galaxies. We find that the number of arcs sensitively depends on the values of α and c_{norm}. In addition, the number of arcs, if divided by the corresponding number of halos, is almost insensitive to the underlying cosmological parameters. Therefore, they prove to be a powerful discriminator of a family of halo density profiles suggested by recent numerical simulations.

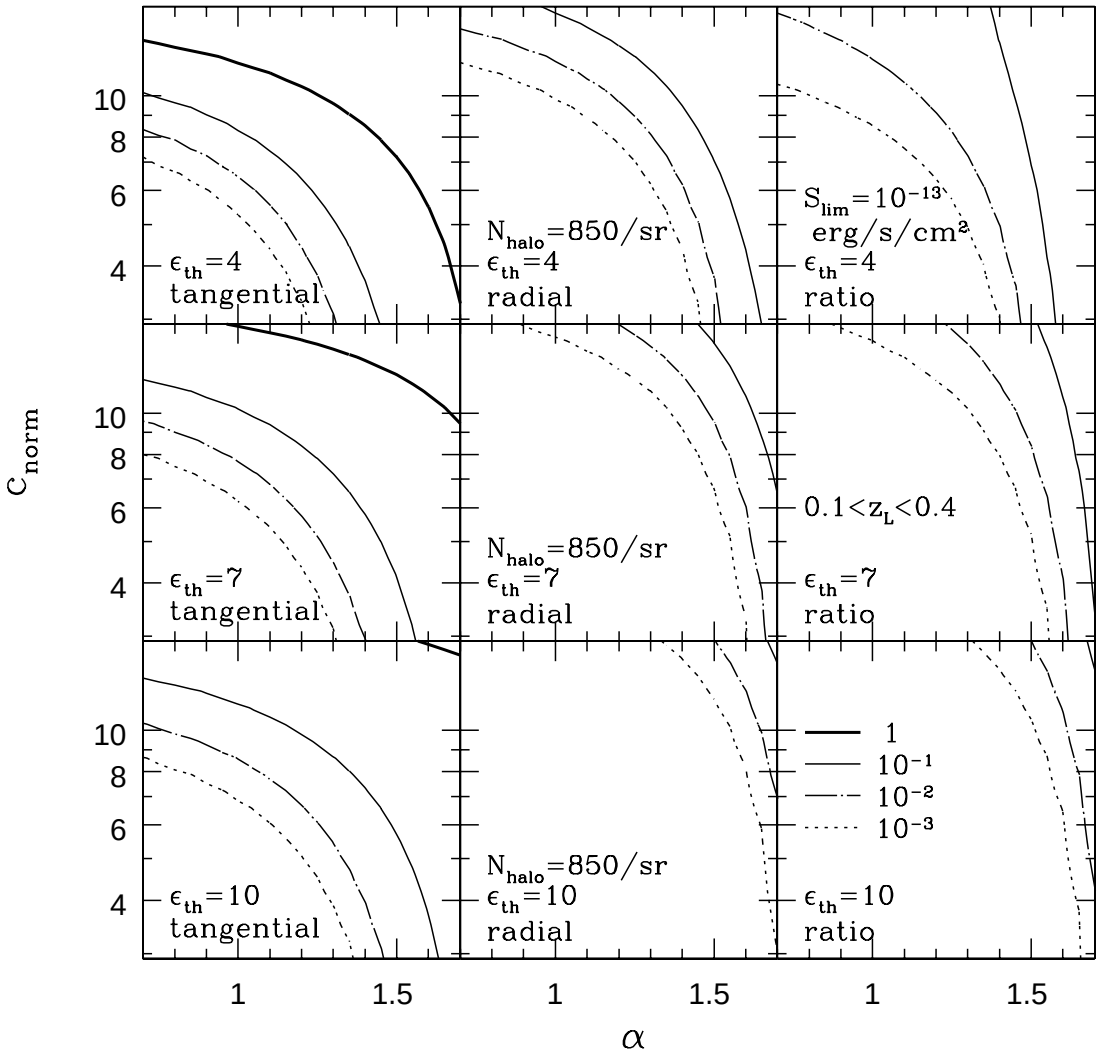

FIG. 6.—Effect of different thresholds of the length-to-width ratio on the arc statistics for X-ray flux–limited samples with $S_{lim} = 10^{-13}$ ergs s^{-1} cm^{-2} in the LCDM model: $\epsilon_{th} = 4$ (*top*), $\epsilon_{th} = 7$ (*middle*), and $\epsilon_{th} = 10$ (*bottom*). The contour levels are the same as Fig. 4.

Molikawa & Hattori (2001) propose using the number ratio of tangential and radial arcs W to probe the density profile. We confirm that the ratio remains a useful *statistical* measure even after taking account of the average over the cosmological mass function, the redshift evolution, mass dependence, and the probability distribution of the concentration parameter. We also show that the effects of finite source size are important even in the case of the number ratio W. On the other hand, W is mainly sensitive to the inner slope α, and we argue that complementary information on c_{norm} can be obtained by combining the number of tangential arcs per halo.

Our major conclusion, that the cosmological model dependence of arc statistics is much weaker than the profile parameters, seems inconsistent with the claim by Bartelmann et al. (1998). We note, however, that they use different values of the concentration parameter for different cosmological models. Thus, we suspect that the claimed cosmological model dependence actually reflects the sensitivity to the concentration parameter that we discussed at length.

The preliminary comparison with observations suggests that dark matter halos should have steep inner profiles. This comparison, however, is inconsistent with the mass profile of Cl 0024+1654 reconstructed from gravitational lensing images (Tyson et al. 1998) and with the rotation curves of low surface brightness galaxies, which indicate a flat core (Salucci & Burkert 2000; de Blok et al. 2001). Therefore, it is still premature to draw any strong conclusions about, e.g., a self-interacting dark matter model (Spergel & Steinhardt 2000) at this point, and it is important to put many constraints on the halo density profile from separate and independent analyses.

Certainly we have to improve the present methodology by taking account of more realistic effects. First, Bartelmann, Steinmetz, & Weiss (1995) pointed out that the number of arcs becomes significantly larger if the intrinsic ellipticity distribution of source galaxies is taken into account. This will increase the numbers of both tangential and radial arcs. Thus, these quantitative estimates are important. Secondly, we neglect the effects of the galaxies in clusters. In particular, the central cD galaxies move the radial arc closer to the center (Miralda-Escudé 1995) and will affect, especially, the number of radial arcs. On the other hand, the effect of cluster galaxies seems to be small and enhances the number of arcs only $\lesssim$15% (Flores, Maller, & Primack 2000; Meneghetti et al. 2000), although they may affect the number of tangential and radial arcs

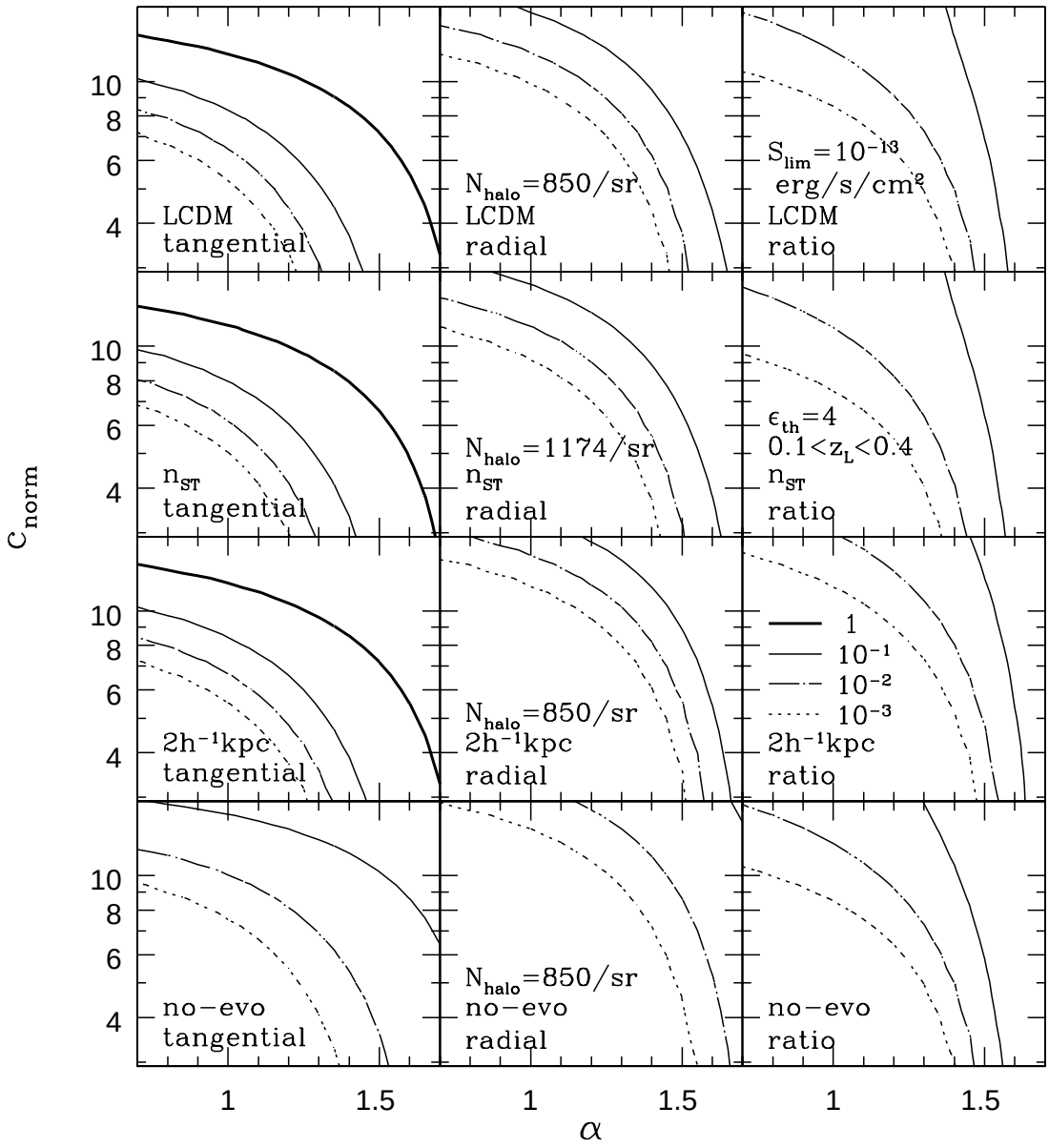

FIG. 7.—Sensitivity of our predictions on the adopted model parameters for X-ray flux–limited samples with $S_{\rm lim} = 10^{-13}$ ergs^{-1} s^{-1} cm^2 in the LCDM model. The first row displays our fiducial model (same as in Fig. 4). The second row adopts $n_{\rm ST}$ (eq. [29]) instead of $n_{\rm PS}$ (eq. [26]) for the mass function of halos. The third row adopts $\eta_{\rm crit} = 2\ h^{-1}$ kpc instead of $\eta_{\rm crit} = 1\ h^{-1}$ kpc for the cutoff size of source galaxies. The fourth row assumes no evolution in the luminosity function.

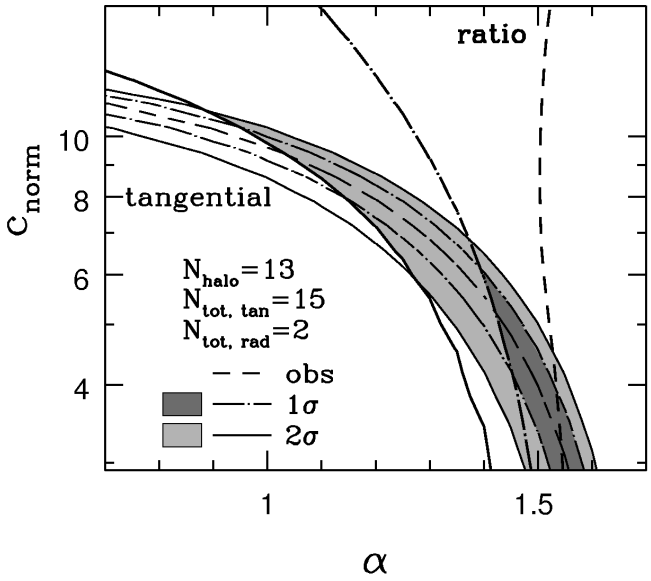

FIG. 8.—Tentative constraints on α and $c_{\rm norm}$ from a sample of 13 clusters with $0.1 < z < 0.4$ and $S_{\rm lim} = 10^{-12}$ ergs s^{-1} cm^{-2}. The LCDM model is assumed. Dashed lines represent the relations of α and $c_{\rm norm}$ that reproduce the observed number for tangential arcs and the number ratio of radial to tangential arcs. Dark- and light-shaded regions indicate the allowed regions combined from the two constraints taking account of the 1 and 2 σ statistical errors, respectively.

differently. Finally, deviations from spherical symmetry of lens halos change the number of arcs (Bartelmann 1995; Molikawa et al. 1999), which will increase the number of tangential arcs and decrease the number of radial arcs (Molikawa & Hattori 2001). Therefore, this effect is certainly important in discussing the number ratio W as well as the total number of arcs. We plan to incorporate these effects in a systematic and quantitative fashion, which will be reported separately.

We thank Takeshi Chiba, Takashi Hamana, and Ryuichi Takahashi for useful discussions and Xiang-Ping Wu for his instructive comments. We also thank an anonymous referee for many useful comments that improved the earlier manuscript. This research was supported in part by a Grant-in-Aid from the Ministry of Education, Science, Sports and Culture of Japan (07CE2002) to RESCEU.

REFERENCES

Bartelmann, M. 1995, A&A, 299, 11
Bartelmann, M., Huss, A., Colberg, J. M., Jenkins, A., & Pearce, F. R. 1998, A&A, 330, 1
Bartelmann, M., Steinmetz, M., & Weiss, A. 1995, A&A, 297, 1
Broadhurst, T. J., Ellis, R. S., & Shanks, T. 1988, MNRAS, 235, 827
Broadhurst, T., Huang, X., Frye, B., & Ellis, R. 2000, ApJ, 534, L15
Bullock, J. S., Kolatt, T. S., Sigad, Y., Somerville, R. S., Kravtsov, A. V., Klypin, A. A., Primack, J. R., & Dekel, A. 2001, MNRAS, 321, 559
de Blok, W. J. G., McGaugh, S. S., Bosma, A., & Rubin, V. C. 2001, ApJ, 552, L23
Flores, R. A., Maller, A. H., & Primack, J. R. 2000, ApJ, 535, 555
Folkes, S., et al. 1999, MNRAS, 308, 459
Fukushige, T., & Makino, J. 2001, ApJ, 557, 553
Hamana, T., & Futamase, T. 1997, MNRAS, 286, L7
Hattori, M., Watanabe, K., & Yamashita, K. 1997, A&A, 319, 764
Hoffman, Y., & Shaham, J. 1985, ApJ, 297, 16
Jenkins, A., Frenk, C. S., White, S. D. M., Colberg, J. M., Cole, S., Evrard, A. E., Couchman, H. M. P., & Yoshida, N. 2001, MNRAS, 321, 372
Jing, Y. P. 2000, ApJ, 535, 30
Jing, Y. P., & Suto, Y. 2000, ApJ, 529, L69
Keeton, C. R., & Madau, P. 2001, ApJ, 549, L25
King, C. R., & Ellis, R. S. 1985, ApJ, 288, 456
Kitayama, T., Sasaki, S., & Suto, Y. 1998, PASJ, 50, 1
Kitayama, T., & Suto, Y. 1996, ApJ, 469, 480
———. 1997, ApJ, 490, 557
Li, L. X., & Ostriker, J. P. 2001, ApJ, submitted (astro-ph/0010432)
Łokas, E. L., & Hoffman, Y. 2000, ApJ, 542, L139
Luppino, G. A., Gioia, I. M., Hammer, F., Le Fèvre, O., & Annis, J. A. 1999, A&AS, 136, 117
Meneghetti, M., Bolzonella, M., Bartelmann, M., Moscardini, L., & Tormen, G. 2000, MNRAS, 314, 338
Meneghetti, M., Yoshida, N., Bartelmann, M., Moscardini, L., Springel, V., Tormen, G., & White, S. D. M. 2001, MNRAS, 325, 435
Miralda-Escudé, J. 1993a, ApJ, 403, 497
———. 1993b, ApJ, 403, 509
———. 1995, ApJ, 438, 514
Molikawa, K., & Hattori, M. 2001, ApJ, in press
Molikawa, K., Hattori, M., Kneib, J.-P., & Yamashita, K. 1999, A&A, 351, 413
Moore, B., Quinn, T., Governato, F., Stadel, J., & Lake, G. 1999, MNRAS, 310, 1147
Nakamura, T. T., & Suto, Y. 1997, Prog. Theor. Phys., 97, 49
Navarro, J. F., Frenk, C. S., & White, S. D. M. 1996, ApJ, 462, 563
———. 1997, ApJ, 490, 493
Nusser, A., & Sheth, R. K. 1999, MNRAS, 303, 685
Press, W. H., & Schechter, P. 1974, ApJ, 187, 425
Salucci, P., & Burkert, A. 2000, ApJ, 537, L9
Schneider, P., Ehlers, J., & Falco, E. E. 1992, Gravitational Lenses (New York: Springer)
Shapiro, P. R., & Iliev, I. T. 2000, ApJ, 542, L1
Sheth, R. K., & Tormen, G. 1999, MNRAS, 308, 119
Spergel, D. N., & Steinhardt, P. J. 2000, Phys. Rev. Lett., 84, 3760
Suto, Y., Yamamoto, K., Kitayama, T., & Jing, Y. P. 2000, ApJ, 534, 551
Syer, D., & White, S. D. M. 1998, MNRAS, 293, 337
Takahashi, R., & Chiba, T. 2001, ApJ, submitted (astro-ph/0106176)
Tyson, J. A., Kochanski, G. P., & Dell'Antonio, I. P. 1998, ApJ, 498, L107
van den Bosch, F. C., Robertson, B. E., Dalcanton, J. J., & de Blok, W. J. G. 2000, AJ, 119, 1579
Williams, L. L. R., Navarro, J. F., & Bartelmann, M. 1999, ApJ, 527, 535
Wu, X. P., & Chiueh, T. 2001, ApJ, 547, 82
Wu, X. P., & Hammer, F. 1993, MNRAS, 262, 187
Wu, X. P., & Mao, S. 1996, ApJ, 463, 404
Wu, X. P., & Xue, Y. J. 2000, ApJ, 529, L5
Wyithe, J. S. B., Turner, E. L., & Spergel, D. N. 2001, ApJ, 555, 504